Journal of Catalysis 328 (2015) 130–138

Contents lists available at ScienceDirect

Journal of Catalysis

journal homepage: www.elsevier.com/locate/jcat

Effect of support surface treatment on the synthesis, structure, and performance of Co/CNT Fischer–Tropsch catalysts ☆

Thomas O. Eschemann [a,1], Wouter S. Lamme [a,1], Rene L. Manchester [a,1], Tanja E. Parmentier [a,b,1], Andrea Cognigni [b], Magnus Rønning [b,*], Krijn P. de Jong [a,*,1]

[a] Inorganic Chemistry and Catalysis, Debye Institute for Nanomaterial Science, Utrecht University, P.O. Box 80083, 3508 TB Utrecht, The Netherlands
[b] Department of Chemical Engineering, Norwegian University of Science and Technology (NTNU), NO-7491 Trondheim, Norway

ARTICLE INFO

Article history:
Received 15 September 2014
Revised 18 November 2014
Accepted 11 December 2014

Keywords:
Fischer–Tropsch
Carbon nanotubes (CNT)
Cobalt
Impregnation
Solvent effects
Surface functionalization
Gas-phase oxidation

ABSTRACT

We report the preparation of supported cobalt catalysts (9 wt% Co) on untreated (CNT) and surface-oxidized (CNT-ox) carbon nanotube materials by incipient wetness impregnation with solutions of cobalt nitrate in water, ethanol, or 1-propanol. The results show that by a judicious selection of solvent and drying method, similar cobalt oxide particle sizes in the range of 4–5 nm on CNT and CNT-ox materials were obtained for the fresh catalysts. Cobalt particles supported on unfunctionalized CNT showed higher initial activities and C_{5+}-selectivities than catalysts on functionalized CNT; however, the former catalysts were more prone to cobalt particle growth due to the lack of anchoring sites. The activities and cobalt particle sizes of catalysts after 60 h on stream revealed for particles larger than 6 nm a turnover frequencies (TOF) of 0.07 s^{-1} for Co/CNT and 0.03 s^{-1} for Co/CNT-ox. *In situ* XAS/XRPD studies showed a similar degree of reduction for the catalysts on untreated and oxidized CNT and the formation of *hcp* cobalt metal on untreated CNT which rationalizes the higher activity and TOF of the Co/CNT catalysts.

1. Introduction

The Fischer–Tropsch synthesis (FTS) comprises the catalytic conversion of synthesis gas into hydrocarbons and is considered a promising process to produce a mixture of long-chain hydrocarbons, which can further be upgraded to ultraclean transportation fuels, chemicals, and lubricants [1–3]. Since synthesis gas can be generated from different sources such as natural gas, shale gas, coal, or biomass, the FTS has awaked interest against the background of souring crude oil prices and geopolitical uncertainties. For the economic prospects of FT plants, good catalyst performance at affordable costs is crucial, making supported cobalt catalysts the material of choice for modern low-temperature Fischer–Tropsch plants based on synthesis gas derived from natural gas [4–8].

Industrially used cobalt catalysts contain both structural and electronic promoters [9–11] and are typically supported on refractory oxides such as alumina, silica, or titania [6,12–15]. Highly active and selective catalysts have been developed [16–21]; however, these support materials often have the disadvantages of limited hydrothermal stability, low reducibility of cobalt oxide to metallic cobalt, or strong metal support interactions (SMSI) [22–25]. Various carbonaceous support materials have been introduced as promising alternatives to overcome these drawbacks, such as activated carbon (AC), carbon spheres (CS), carbon nanofibers (CNF), or carbon nanotubes (CNT) [26–31]. These materials are chemically robust and do not form cobalt-support compounds [32,33]. Commercially available multiwalled carbon nanotubes (MWCNT) as used in this study consist of rolled up graphene sheets that are arranged in a Russian doll fashion, featuring a well-defined structure, a high pore volume, a high specific surface area, and a largely unfunctionalized and thereby hydrophobic surface [33].

In previous work, carbonaceous materials were mostly functionalized prior to being used as support material for metal catalysts, in order to improve the wetting properties for aqueous solutions relevant for metal precursor deposition and to create anchoring sites for the metal nanoparticles [26,34]. Several approaches have been used previously to functionalize the surface of carbonaceous support materials, most importantly liquid-phase

☆ This publication is dedicated to the memory of Haldor Topsøe, whose work in the fields of electron microscopy and synthesis gas generation has been a true inspiration to us in the past decades.

* Corresponding authors. Fax: +31 30 251 1027 (K.P. de Jong).
E-mail addresses: magnus.ronning@ntnu.no (M. Rønning), k.p.dejong@uu.nl (K.P. de Jong).
[1] Visiting address: Inorganic Chemistry and Catalysis, Debye Institute for Nanomaterial Science, Utrecht University, Universiteitsweg 99, 3584 CG Utrecht, The Netherlands.

http://dx.doi.org/10.1016/j.jcat.2014.12.010
0021-9517/

oxidation using nitric acid, sulfuric acid, or mixtures thereof [33,35]. Since these methods often severely damage the catalyst structure, milder methods have been developed, both for liquid-phase and gas-phase functionalization [32,36,37]. Few publications focus on the impact of support functionalization on catalyst structure and performance, and often the conclusions are based on systems with very different metal dispersions or distributions [38–44].

It is the goal of this work to study the influence of support functionalization on the properties of Co/CNT catalysts at comparable cobalt dispersions. While the physicochemical properties of untreated commercially available support material used in this work have been studied in detail before [33], it is the goal of this work to focus on the most important structural changes introduced by the functionalization procedures and their impact on the catalyst synthesis process. Therefore, we used both liquid-phase and gas-phase oxidation [32] to modify the CNT surface properties and to introduce acidic groups. The materials were characterized by means of nitrogen physisorption, transmission electron microscopy, Raman spectroscopy, and acid-base titrations. Supported cobalt catalysts were prepared on these CNT materials using incipient wetness impregnation with different solvents and a drying and heat treatment protocol that has been proven to lead to good distributions of the supported metal particles over the support surface [45,46]. The impact of the chosen materials and methods on dispersion and distribution of cobalt was studied by electron microscopy and X-ray diffraction. The catalysts were then tested under industrially relevant FTS conditions to study trends in activity, selectivity, and stability, while special attention was paid to the extent of reduction under the process conditions using *in situ* XANES.

2. Materials and methods

2.1. Catalyst preparation

Commercially available multiwalled carbon nanotubes (CNT, Baytubes C 150 HP, Bayer Material Science) were functionalized using gas-phase oxidation in a setup as described elsewhere [32]. Typically, 0.4 g of CNT (grain size 75–150 μm) was dried in a sample holder for 2 h at 398 K. Then, a condenser and a round-bottom flask containing about 150 mL nitric acid (65%, Merck) were fitted to the heated sample holder, its design preventing the contact of condensed nitric acid with the sample. Nitric acid was heated to reflux for 0.5–4 h, before the heating mantle was removed. Then, the acid was allowed to cool down while the sample holder was still heated to prevent condensation of any vapors in the sample. Afterward, the oxidized carbon nanotubes (CNT-ox-Xh, X being the duration of oxidation) were dried in a static oven at 393 K overnight. Alternatively, the samples were functionalized using liquid-phase oxidation. Therefore, typically 2 g of CNT was suspended in 40 mL nitric acid (65%, Merck) and heated at 393 K for 2 h. Afterward, the suspension was allowed to cool down and the material was filtered off and washed with water until the pH was close to neutral. The material was then dried in a static oven at 393 K overnight and designated as CNT-LPO-2h.

After drying the support material *in vacuo*, the carbon nanotubes were loaded by incipient wetness impregnation with 1.5 M solutions of cobalt nitrate hexahydrate (p.a., Acros) in water, ethanol, or 1-propanol. The materials were then dried in a static oven at 333 K in air overnight or in a down-flow tubular setup under nitrogen flow at a temperature about 20 K below the boiling point of the solvent used for impregnation. Therefore, the reactor was heated fast to the desired temperature, which was then held for 2 h. To decompose the cobalt precursor, the temperature was then increased to 523 K (2 K/min) and held for 4 h under a flow of nitrogen (GHSV ~6000 h^{-1}). All cobalt loadings for the catalysts prepared were around 9 wt%, assuming Co to be in the form of Co_3O_4. The loadings were calculated by determining the mass of solution added during the impregnation of the catalysts. The catalysts prepared on untreated and oxidized carbon nanotubes were named Co/CNT-solvent or Co/CNT-ox-solvent, respectively, with the solvents deionized H_2O, EtOH (Interchema, >99%), and 1-PrOH (Alfa Aesar, >99.5%) used during the impregnation step.

2.2. Catalyst characterization

Nitrogen physisorption was carried out using a Micromeritics Tristar 3000 setup. Prior to measurements, the samples were degassed at 498 K for 20 h with a ramp of 10 K/min. Physisorption was measured at 77 K from 0 to 0.995 p/p_0. Surface area was estimated using the BET approach, and average pore size distributions were determined from the desorption branches of the isotherms using the BJH method. The micropore volume was approximated using the t-plot method, and total pore volumes were determined from single point adsorption at $p/p_0 = 0.995$.

X-ray powder diffraction (XRD) was performed on a Bruker D2 Phaser with a Co Kα (λ = 1.789 Å) source. Co_3O_4 crystallite size estimation was carried out using the Co_3O_4 peak at 36.8° 2θ with an automatic calculation routine in DiffracEvaluation V2.0 software by Bruker, which is based on the Debye–Scherrer equation.

For transmission electron microscopy (TEM), the support materials or the heat-treated catalysts were carefully ground with a mortar, suspended in ethanol using an ultrasonic bath, and dropped onto a copper TEM grid with holey carbon film. The samples were analyzed using a Tecnai T12 or a Tecnai T20 microscope with electron beam voltages of 120 kV and 200 kV, respectively. Image analysis was carried out with iTEM, the sizes of a at least 150 Co_3O_4 particles were measured, and the average diameter was used to derive an equivalent value for the average metallic cobalt particle size by using the relation $d(Co) = 0.75\ d(Co_3O_4)$. The same relation was used for analyzing the spent catalysts [47].

Temperature-programmed reduction (TPR) was carried out using a Micromeritics Autochem II ASAP 2920. Typically, 50 mg of the sample was dried in a flow of Ar at 393 K for 1 h and then reduced in a flow of H_2/Ar (1:19, v/v) using a ramp of 5 K/min.

Titrations were performed using a Radiometer Analytical TitraLab TIM880 titration manager. Typically, 25–50 mg of the sample was loaded, and 60 mL 0.1 M KCl (aq) was added while stirring. In order to remove dissolved CO_2, the liquid was flushed with nitrogen for 2 min before adding the titrant. The sample was titrated using an aqueous solution containing 0.01 M NaOH and 0.1 M KCl until the pH reached 9 or until the added volume V was 5 mL. The inflection point was found by numerically calculating the first derivative and then applying a second-degree polynomial fit ($y = aV^2 + bV + c$) around the maximum, finding the inflection point by calculating $V_{inflection} = -b/2a$.

Raman spectroscopy was performed with a Kaiser Optical Systems Inc. Raman Spectrometer equipped with a 532 nm laser. Measurements were taken at 50 mW with an exposure time of 7 s and 11 accumulations using Holograms 4.0 software.

Combined *in situ* XANES/XRD studies were performed at the Swiss–Norwegian Beamline (SNBL) at the European Synchrotron Radiation Facility (ESRF), station BM01B. The dried catalysts were diluted with boron nitride (1:1 v/v) and loaded in a quartz capillary with an outer diameter of 1 mm and a wall thickness of 0.02 mm. The bed length was 10 mm, and the catalyst bed was fixed using glass wool. The setup for the *in situ* measurements was described elsewhere [48]. The wavelength used for XRD was 0.4944 Å, and the data were converted to 1.78897 Å (Co Kα) using the software Winplotr. Calibration of the energy of the edge of the XAS spectra

and linear combination fitting was done with the IFEFFIT program Athena. The Co K-edge energy of the reference compound was calibrated by setting the zero crossing of the second derivative to 7709 eV, and the edge energy of the spectra were chosen as a set fraction of the edge step. For the fitting, Co foil and CoO or Co_3O_4 diluted with BN (1:1 *v*/*v*) were used as standards. The first reduction was carried out at 623 K (5 K/min) using a flow of H_2/He (1:3 *v*/*v*). After 5 h at 523 K, the system was cooled to 553 K, and the feed mixture was changed to CO/H_2 (1:2.1 *v*/*v*). The pressure was increased to 15 bar and the temperature to 493 K. These conditions were kept constant for 10 h; afterward, the system was returned to ambient pressure and the setup was flushed with pure H_2. The second reduction step took place at 673 K (5 K/min) for 5 h. Afterward, the temperature was decreased to 553 K and the gas flow was changed to CO/H_2 (1:2.1 *v*/*v*). Again, the pressure was increased to 15 bar and the temperature was set to 473 K, and these conditions were held for another 3 h.

2.3. Fischer–Tropsch synthesis

Fischer–Tropsch synthesis was carried out in a 16 reactor catalytic testing setup (Flowrence, Avantium). The catalysts (75–150 μm) were diluted with SiC (200 μm) to arrive at the same amount of Co in every reactor, giving a catalyst bed volume of 200 μL. The catalysts were dried in a flow of He at 373 K for 2 h and then reduced *in situ* in a flow of H_2/He (1:3 *v*/*v*) at 623 K (8 h, ramp 1 K/min). Subsequently, the reactors were cooled to 453 K and pressurized to 20 bar under a flow of H_2. After switching to H_2/CO (2:1 *v*/*v*), the temperature was increased to 493 K (1 K/min), and the products were analyzed using online gas chromatography (Agilent 7890A). The permanent gases were separated on a ShinCarbon ST (#19043) column and quantified against He as an internal standard using a TCD detector. CO conversions were calculated as $X_{CO} = (mol_{CO\ in} - mol_{CO\ out})/mol_{CO\ in}$. Hydrocarbons (C1–C9) were separated on an Agilent J&W PoraBOND Q column, detected using an FID detector and quantified against the TCD signal of the internal standard He. Selectivities to the lower hydrocarbon fractions S_{CX} were calculated from converted CO and the corresponding yields as $S_{CX} = Y_{CX}/(mol_{CO\ in} - mol_{CO\ out})$. The selectivities to products with 5 and more carbon atoms were calculated from the yields to lower hydrocarbons as $S_{C5+} = 1 - S_{C1-C4}$. Stable CO conversions and hydrocarbon selectivities were reached after about 50 h on stream and were between 25% and 35%. Activities are reported as cobalt-time yields (CTY, $mol_{CO}/(g_{Co}\cdot s)$). At the end of the catalytic testing experiment, the waxes in the pores of the catalysts were stripped off the catalysts for 12 h under a flow of H_2 at 473 K, and subsequently, the reactors were cooled down to room temperature under a flow of Ar. When removing the catalysts from the reactors, these were exposed to air prior to further characterization by TEM. Although the purity of the CNT material was greater than 99% C, the support material contains small amounts of residual growth catalyst from the industrial manufacturing process, which might have an effect on the catalytic properties. Therefore, the activity of the blank support material was also tested in the catalytic experiments, but it was found to be negligible.

3. Results and discussion

3.1. Characterization of the support materials

Transmission electron microscopy (TEM) imaging (Fig. 1) was used to obtain information on the local structural changes in the carbon nanotubes upon functionalization. While the untreated CNT show smooth parallel rolled up graphene sheets with disordered deposits both inside and outside as described in the literature [33], distinct differences can be found in the modified nanotubes. The materials oxidized by gas-phase oxidation show a roughening of the nanotube surface, while the structure otherwise seems intact. For the CNT oxidized by liquid-phase oxidation, a severe distortion of the original structure is noted as the surface was roughened and few parallel graphene sheets are observed.

The number of acidic groups on the functionalized materials was determined by acid-base titrations. Using this method, for the unfunctionalized materials, no acidic groups were found (Fig. 2). The samples treated in the gas phase show that the number of acid sites increased with short oxidation times as expected, while longer times did not lead to significantly higher degrees of functionalization, a behavior that has been observed before. Note that the number of acid sites introduced for longer oxidation times was very similar to the result for liquid-phase-oxidized nanotubes (0.40 mmol/g) [32,36]. It should be noted that for both the untreated and functionalized CNT, the amount of oxygen-containing groups may be higher than the amount of acid sites determined by titration. For more accurate methods to quantitatively determine the amount of oxygen-containing groups, high-resolution XPS studies have been carried out successfully before [49,50].

The degree of surface functionalization also played a key role in the wetting properties of the materials with different solvents. While oxidized CNT were wetted by water, ethanol, or 1-propanol, the untreated materials floated on water indicating poor wetting properties. The untreated CNT materials, however, were wetted properly by ethanol or 1-propanol.

Nitrogen physisorption on untreated and oxidized samples showed very similar adsorption–desorption curves (see Supporting information, Fig. S3) that can be best described as IUPAC type IV isotherms with hysteresis at $p/p_0 > 0.9$. A slight increase of pore volume and BET surface area was noted for the gas-phase-oxidized CNT. (Table 1) The similarities in porosity suggest that the overall

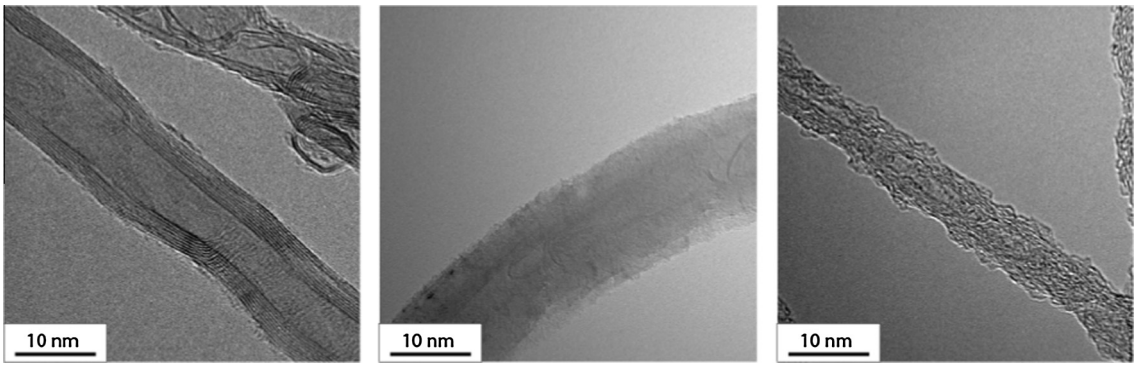

Fig. 1. Representative TEM images of untreated (left), 2 h gas-phase-oxidized (center), and 2 h liquid-phase-oxidized (right) carbon nanotubes.

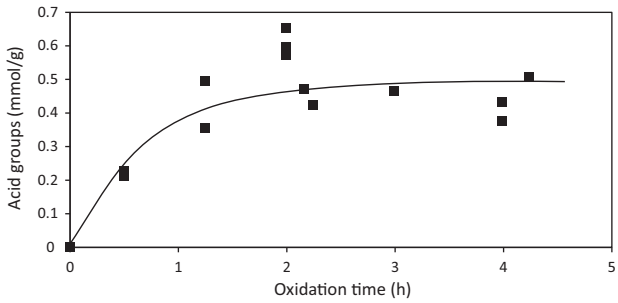

Fig. 2. Number of acidic groups on the CNT surface for different gas-phase oxidation times. The line through the points has been drawn to guide the eye.

Table 1
Influence of oxidation treatments on the porosity of the carbon support materials.

Support material	BET area (m^2/g)	Total pore volume (mL/g)
CNT	200	1.2
CNT-GPO-2h	250	1.4
CNT-LPO-2h	270	1.1

Table 2
Raman data obtained for untreated and oxidized carbon nanotubes.

Support material	D_1 band FWHM (cm^{-1})	G band FWHM (cm^{-1})	I_{D1}/I_G
CNT untreated	59	57	1.2
CNT-GPO-2h	52	44	1.4
CNT-LPO-2h	36	85	39

structure of the gas-phase-oxidized CNT has not been severely affected by the oxidation treatment, which is in line with the observations made with TEM. For liquid-phase-oxidized CNT, a further increase in BET area is observed and the pore volume is found to be a bit lower than the other materials.

Raman spectroscopy was carried out to obtain further information how the different oxidation treatments had affected the CNT (Fig. 3, Table 2). The spectra of the untreated CNT show the typical pattern that has been discussed elsewhere in the literature [33], featuring a distinct band at ~1580 cm^{-1} for the ideal graphitic lattice (G), at ~1340 cm^{-1} for disordered graphitic lattice (A_{1g} symmetry, D_1) and a shoulder on the G peak at ~1620 cm^{-1} that can also be assigned to disordered graphitic lattice (E_{2g} symmetry, D_2) [51]. The relative intensity of the G band decreased for the

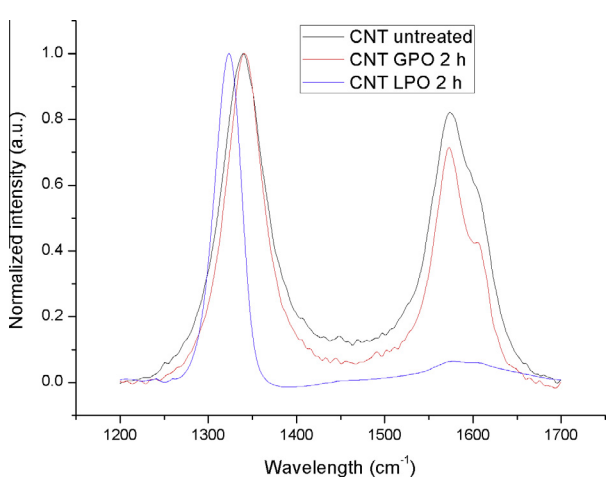

Fig. 3. Raman spectra of untreated and functionalized carbon nanotubes.

Table 3
Co_3O_4 crystallite sizes (nm) determined by XRD line broadening for 9 wt% Co/CNT samples.

Support/solvent	Water	Ethanol	1-Propanol
CNT	6	4	4
CNT-GPO-2h	5	5	3
CNT-LPO-2h	n/a	4	n/a

gas-phase-oxidized sample and its D_2 shoulder becomes more apparent, indicating the increasing degree of disorder in the sample. For liquid-phase-oxidized CNT, the G band disappeared almost completely. The spectra were deconvoluted (for details see Supporting information) using Gaussian functions of the three contributions described above including a contribution of amorphous carbon (D_3) at ~1480 cm^{-1}. The increase of the I_{D1}/I_G ratio is in line with the observations from TEM images and suggests only slight structural distortions when using gas-phase oxidation and severe structural damage for the samples using liquid-phase oxidation. In contrast to what is reported elsewhere in the literature [33], we found that both the D_1 and the G band became narrower going from the untreated sample to the gas-phase-oxidized CNT and to the liquid-phase-oxidized sample. Also, a distinct redshift of the D_1 band to ~1320 cm^{-1} is observed for the LPO sample. These effects have been interpreted as graphitic domains being smaller for related materials [52] and is in line with the other observations of the structural distortion.

3.2. Characterization of the heat-treated catalysts

XRD line broadening analysis was carried out on the heat-treated CNT-supported catalysts to estimate the size of the Co_3O_4 crystallites. (Table 3) The results show relatively small cobalt oxide crystallites of 3–6 nm with little difference between the catalysts prepared on untreated and oxidized CNT. For both the catalysts on untreated and on oxidized CNT, the largest crystallite sizes were found for the catalysts impregnated with aqueous solutions, while smaller crystallites were detected for impregnations with ethanol or propanol.

TEM particle size analysis results of the heat-treated catalysts were in good accordance with the values deduced from XRD line broadening analysis (see also Table 5). Moreover, the images provided indications on the nanoscale distribution of the cobalt oxide particles over the CNT. The catalysts prepared by aqueous impregnations showed clusters of about 20 nm, while less clustering was observed for catalysts prepared by impregnations using cobalt nitrate solutions in ethanol and quite uniform distributions for the catalysts impregnated with solutions of 1-propanol (Fig. 4). When comparing the catalysts supported on untreated CNT with their counterparts on oxidized CNT, little difference in terms of cobalt oxide clustering was observed (Fig. 5). These results indicate that the solvent surface tension effects during drying have a larger impact than wetting of the support. In other words, if wetting suffices, then surface tension effects dominate in agglomeration during drying. This finding is nicely in line with the elegant *in situ* TEM studies of Crozier et al. [53] comparing nickel nitrate distributions on silica showing that water as solvent led to more clustering than ethanol as solvent.

The reducibility of the catalysts was studied by temperature-programmed reduction (TPR). Similar patterns were found for all supported cobalt catalysts on untreated and oxidized CNT (see Supporting information, Fig. S4). The patterns showed hydrogen uptake at ~473 K, indicating the presence of residual cobalt nitrate, and two broad peaks at ~573 K and 673 K, resembling the typical two-step reduction pattern, that is of Co_3O_4 to CoO followed by

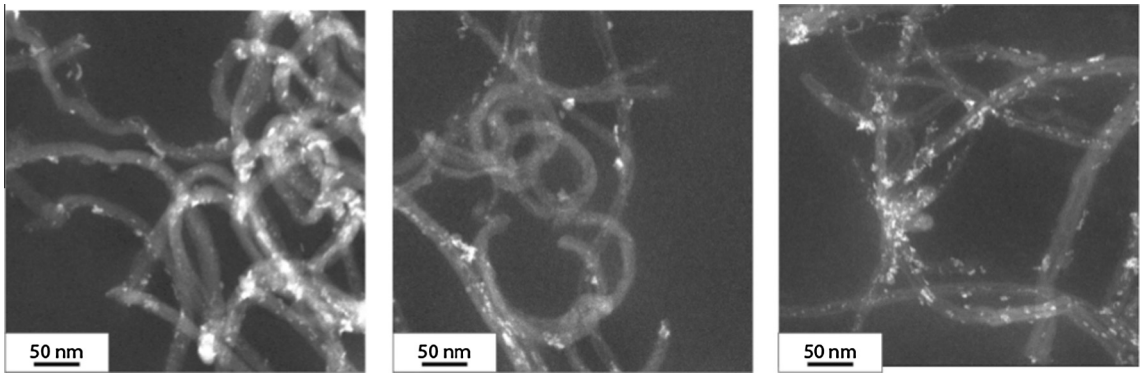

Fig. 4. Representative STEM-HAADF images showing clustering of cobalt oxide particles for untreated CNT support impregnated with aqueous solutions (left: Co/CNT-H_2O), a more homogeneous distribution for catalysts prepared by impregnation with solutions of cobalt nitrate in ethanol (middle, Co/CNT-EtOH), and uniform distribution when using isopropanol as solvent (right, Co/CNT-PrOH).

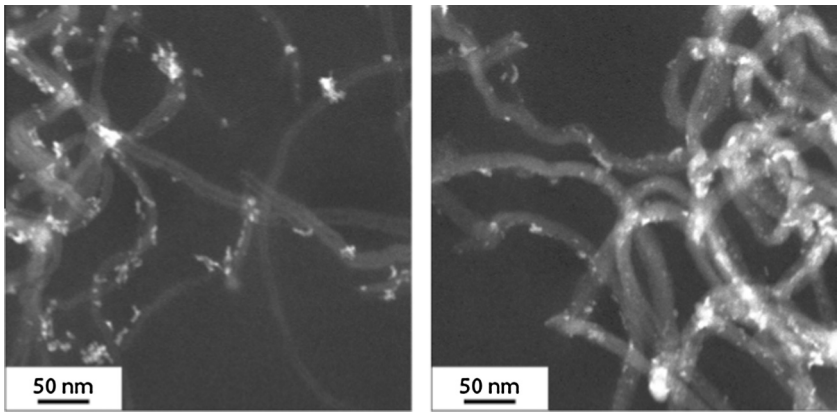

Fig. 5. Representative STEM-HAADF images showing similar cobalt oxide particle distributions for propanol-impregnated catalysts on untreated support (left: Co/CNT-PrOH) and on oxidized support (right: Co/CNT-GPO-PrOH).

reduction of CoO to metallic cobalt [9]. It can be seen that all reduction peaks in the sample supported on oxidized CNT had shifted to higher temperatures, indicating a reduction of cobalt oxide impaired by the presence of the functional groups, which has been reported before [40,54]. A quantification of the TPR data to determine the degree of reduction was difficult, since the hydrogen uptake from the reduction of cobalt oxide is likely to overlap with hydrogen consumption from gasification of the support.

3.3. Fischer–Tropsch synthesis and in situ characterization

The results from catalytic testing at industrially relevant conditions revealed significant differences for the performance of the catalysts. All catalysts supported on untreated CNT showed distinctly higher CTY than their counterparts supported on gas-phase-oxidized or liquid-phase-oxidized CNT (Fig. 6). For both series of cobalt catalysts supported on untreated and on gas-phase-oxidized CNT, the materials impregnated with aqueous solutions showed the lowest activity, while higher activities were found for the systems impregnated with solutions of cobalt nitrate in alcohols. In the case of catalysts supported on oxidized CNT, the catalysts impregnated with ethanol and 1-propanol displayed the same activity, whereas for catalysts on untreated CNT, the systems impregnated with ethanol showed superior activity. Regarding the selectivity to higher hydrocarbons, significantly higher C_{5+}-selectivities were found for the catalysts on untreated CNT (88–91%) than for the catalysts on gas-phase-oxidized CNT (82–86%) and for the catalysts on liquid-phase-oxidized CNT (68%),

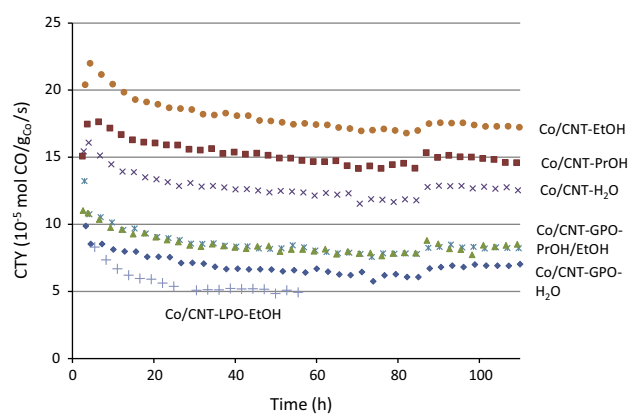

Fig. 6. Cobalt-time yields (CTY) for CNT-supported cobalt catalysts, Fischer–Tropsch synthesis at 20 bar, 493 K, H_2/CO 2.0 v/v, GHSV ~2000 h^{-1}.

although it should be mentioned that the CO conversions for the catalysts on untreated CNT were higher than for the ones supported on gas-phase-oxidized CNT and liquid-phase-oxidized CNT (Table 4). A possible explanation is that for the untreated Co/CNT catalyst, the α-olefins primary products adsorb on the hydrophobic CNT surface, thereby invoking readsorption on cobalt favoring additional chain growth. This readsorption step can be hampered by the presence of polar functional groups. For the surface-oxidized Co/CNT-GPO catalysts, the support surface is

Table 4
Selectivity data for Co/CNT catalysts studied, 20 bar, 493 K, H_2/CO 2.0, GHSV ~2000 h^{-1}, 60 h on stream.

Catalyst	X_{CO}	S_{C1} (wt%)	S_{C2-C4} (wt%)	S_{C5+} (wt%)
Co/CNT-H_2O	29	4	5	91
Co/CNT-EtOH	42	5	5	90
Co/CNT-PrOH	37	6	6	88
Co/CNT-GPO-H_2O	16	11	7	82
Co/CNT-GPO-EtOH	21	11	7	82
Co/CNT-GPO-PrOH	20	10	7	83
Co/CNT-LPO-EtOH[a]	18	19	12	69

[a] Data for Co/CNT-LPO-EtOH after 50 h on stream.

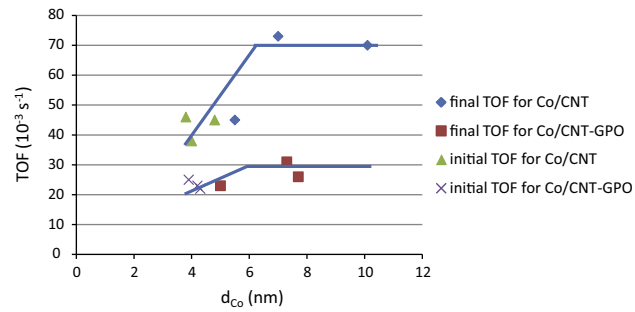

Fig. 7. Initial and final TOF as a function of equivalent cobalt particle sizes. The lines are drawn as a guide to the eye.

expected to have a stronger interaction with polar molecules such as water. If water is preferably adsorbed on the surface, α-olefin readsorption can be inhibited leading to a reduced C_{5+}-selectivity [55]. Similar effects have also been discussed for Co/Al_2O_3 catalysts with different alumina phases where the C_{5+}-selectivity was found to be lower for catalysts supported on alumina phases with higher Lewis acidities [56,57]. We note that except for Co/CNT-LPO and Co/CNT-H_2O, the measured C_{5+}-selectivities were found to correlate with CO conversion (see Supporting information, Fig. S6). However, the measured differences in C_{5+}-selectivities related to the differences in CO conversion ($\Delta S_{C5+}/\Delta X_{CO} \sim 0.4$) are distinctly higher than those reported elsewhere in the literature (e.g. $\Delta S_{C5+}/\Delta X_{CO} \sim 0.1$ for Co/Al_2O_3 [58]).

In order to understand the reasons for the different activities and selectivities, the Co particle sizes before and after the catalytic experiments were determined by TEM. The results (Table 5) showed that the extent of average particle growth correlated with the degree of nanoparticle clustering found for the fresh catalysts (Fig. 5). While initially the cobalt particle sizes in the catalysts were found to be very similar for all systems studied, the clustering in catalysts prepared by impregnations with aqueous solutions led to more severe particle growth and loss of metallic surface area during reduction and Fischer–Tropsch synthesis, explaining the superior activity of catalysts prepared with impregnation using organic solvents.

The turnover frequencies (TOF final) based on the FT activity after 60 h (Fig. 7), and the cobalt particle sizes of the used catalysts for the catalysts supported on untreated CNT were significantly higher than the TOF final found for the catalysts supported on gas-phase-oxidized CNT. The same trend is observed for the initial turnover frequencies based on the particle sizes of the fresh catalysts. This indicates that the activity differences cannot be exclusively explained with differences in the active metal surface area. The fact that the activity for Co/CNT-PrOH was lower than that of Co/CNT-EtOH is rationalized by the fact that the average particle size of the material impregnated with 1-propanol was lower than the critical particle size of ~6 nm, below which the turnover frequency in FT decreases sharply [17]. This also holds for samples prepared on oxidized CNT using 1-propanol as a solvent. Also, all fresh catalysts feature cobalt particle sizes below 6 nm and show lower initial turnover frequency values, underlining the importance of particle size effects (Table 5, Fig. 7).

Considering the results of the TEM particle size analysis and the turnover frequency calculations, the performance differences between the catalysts supported on untreated CNT and their counterparts supported on oxidized CNT is unlikely to arise from differences in dispersion of cobalt. Since the extent of reduction could not be determined from the TPR experiments, *in situ* XANES and XRD were used to probe the chemical nature of cobalt during process conditions. The results showed different reduction rates (Fig. 8) for a catalyst on untreated CNT compared to a catalyst on oxidized CNT. While for the catalyst supported on untreated CNT, the reduction of Co_3O_4 to CoO came to completion after 40 min, there was still Co_3O_4 present for the catalyst supported on oxidized CNT after 80 min. This is in line with the TPR results indicating a hampered reduction for the catalysts supported on oxidized CNT, however, after 2 h, Co_3O_4 was fully reduced and the amounts of CoO and Co formed were very similar.

The extent of reduction was further determined during Fischer–Tropsch synthesis at conditions similar to the catalytic results reported above (Fig. 9). After about 8 h, a steady state was reached and the degree of reduction was found to be 73% for the material on untreated CNT and 81% for the catalysts supported on oxidized CNT.

A second reduction at a higher temperature (673 K) and pressure (5 bar) was carried out, which led to a higher extent of reduction for both catalysts. Under these conditions, the degree of reduction was found to be 84% for the catalyst on untreated CNT and 86% for the system on oxidized CNT. In the second Fischer–Tropsch synthesis cycle (Fig. S5), the degree of reduction was found to be very similar for the two catalysts studied, 89% metallic Co was found for Co/CNT-PrOH, while 87% metallic Co was found for Co/CNT-ox-PrOH (Supporting information, Figs. S5 and S6).

The *in situ* XRD studies (Fig. 10) performed during the first reduction step showed the disappearance of the Co_3O_4 peaks at 39°, 67°, and 74° 2θ in the course of time and the arising of CoO

Table 5
Equivalent cobalt particle sizes (calculated from average TEM Co_3O_4 particle sizes using the relation $d_{Co} = d_{Co3O4} * 0.75$) of fresh and spent Co/CNT catalysts and cobalt-time yields at 60 h on stream. Initial TOF values are based on the equivalent cobalt particle sizes of the fresh catalysts and the initial data points in the catalytic testing. CTY and TOF final are based on the catalytic performance after ~60 h and based on the cobalt particle sizes of the spent catalysts.

Catalyst	d_{Co} fresh (nm)	d_{Co} spent (nm)	CTY (10^{-5} $mol_{CO}/(g_{Co} * s)$)	TOF initial (10^{-3} s^{-1})	TOF final (10^{-3} s^{-1})
Co/CNT-H_2O	4.8	10.1	13	45	70
Co/CNT-EtOH	3.8	7.0	16	46	73
Co/CNT-PrOH	4.0	5.5	18	38	45
Co/CNT-GPO-H_2O	4.3	7.7	7.8	22	26
Co/CNT-GPO-EtOH	3.9	7.3	8.9	25	31
Co/CNT-GPO-PrOH	4.2	5.0	8.9	23	23
Co/CNT-LPO-EtOH	3.6	n/a	5.0	n/a	n/a

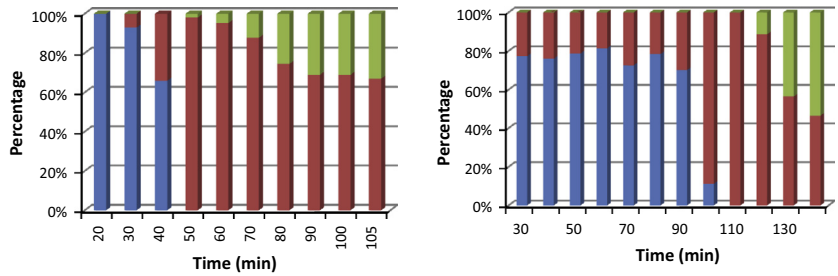

Fig. 8. Phase composition of Co/CNT-PrOH (left) and Co/CNT-ox-PrOH (right) during reduction in a flow of He/H_2 (3.0 *v*/*v*) at 623 K (5 K/min), 1 bar, Co_3O_4 (blue), CoO (red), Co (green). (For the interpretation of the references to color in this figure legend, the reader is referred to the Web version of this article.)

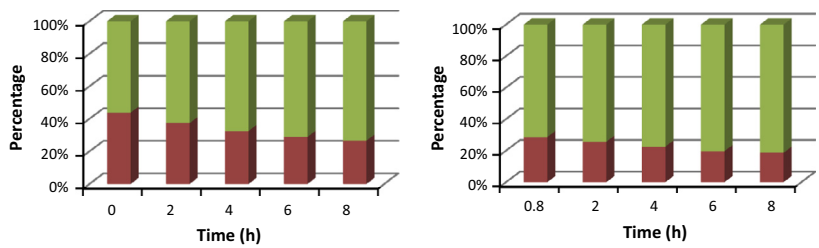

Fig. 9. Phase composition of Co/CNT-PrOH (left) and Co/CNT-ox-PrOH (right) during Fischer–Tropsch synthesis at 493 K, 15 bar, H_2/CO 2.1 *v*/*v*, CoO (red), Co (green). (For the interpretation of the references to color in this figure legend, the reader is referred to the Web version of this article.)

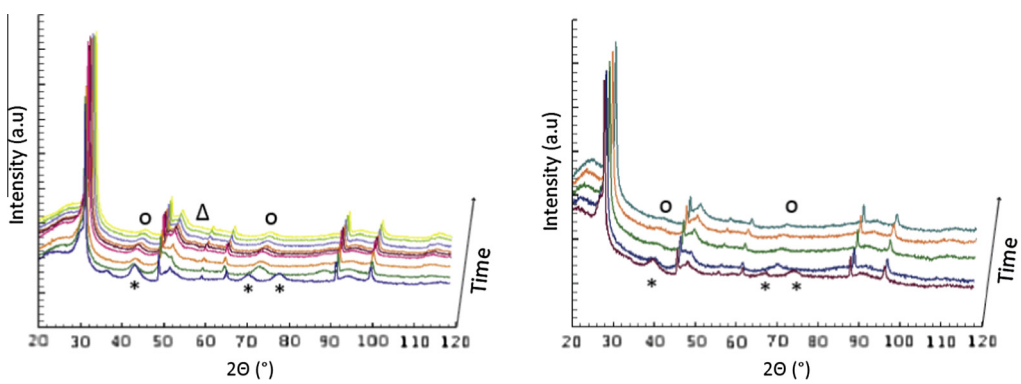

Fig. 10. Diffractograms obtained from *in situ* XRD studies during the first reduction step of a Co/CNT-PrOH (left) and Co/CNT-GPO-PrOH (right) catalyst. Note the disappearance of Co_3O_4 (∗) and the appearance of CoO (o) for both catalysts, while a small peak for hcp Co (Δ) at 54° 2θ is only observed for Co/CNT-PrOH. Conditions: 1 bar, 623 K, H_2/He 1:3 *v*/*v*, diffractograms were recorded every hour during the reduction.

peak at 70° 2θ. For the catalyst supported on untreated CNT, the appearance of a peak at 55° 2θ was observed, indicating the formation of *hcp* Co, while this peak was not found for the catalyst on oxidized CNT. Since *hcp* Co is known to be more active in FTS than *fcc* Co [59,60], these findings might (partly) explain the differences observed for the activities of the catalysts studied in this work.

In order to compare the thermal stability between the catalysts supported on untreated and oxidized CNT, some catalysts were exposed to higher temperatures in several steps, before returning to the Fischer–Tropsch synthesis temperature of 493 K, where the catalyst performance was compared to that of the catalysts that had not been exposed to temperatures higher than 493 K (Fig. 11). The results showed that the activity increased stepwise with increasing the temperature as expected. Upon returning to the original synthesis temperature, however, only the catalyst supported on oxidized CNT returned to its original activity, while the catalyst supported on untreated CNT fell short. After the exposure

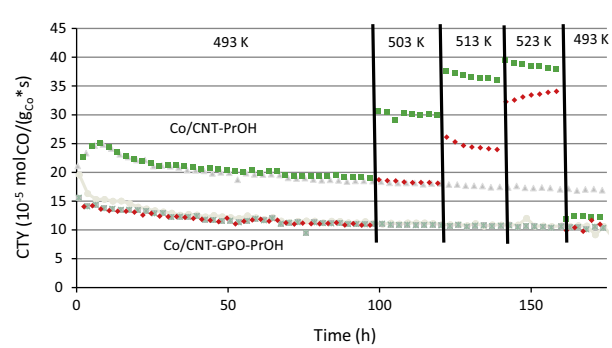

Fig. 11. Cobalt-time yields (CTY) for CNT-supported cobalt catalysts, Fischer–Tropsch synthesis carried out at 20 bar, 493/503/513/523/493 K, H_2/CO 2.0 *v*/*v*, GHSV ~2000 h^{-1}. The gray curves refer to the catalysts that have been exposed to 493 K for the whole duration of the experiment.

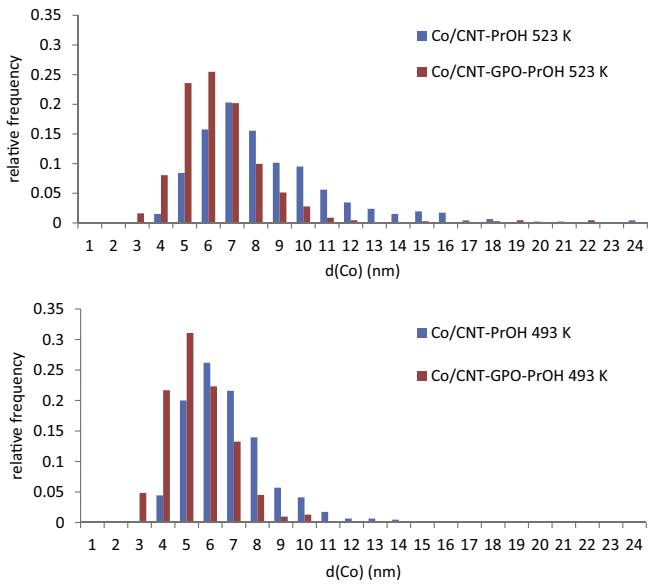

Fig. 12. TEM Particle size distributions for catalysts exposed to 523 K (top) and 493 K (bottom).

to higher temperatures, the catalyst on untreated CNT only showed a slightly higher activity than its counterpart on oxidized CNT.

TEM studies of the spent catalysts showed similar particle size distributions for the catalysts on untreated and oxidized CNT that were used for FTS at 493 K only. For the catalysts exposed to higher temperatures, distinctly more particles greater than 10 nm were found for the catalysts on untreated CNT, while the histogram for the catalyst on oxidized CNT was similar to the one found for exposition to lower temperatures only (Fig. 12).

4. Conclusions

Gas-phase oxidation using nitric acid vapors was used as a versatile route to introduce functional groups on carbon nanotube (CNT) surfaces without severely damaging the overall porous and crystalline structure of the material. The oxidized CNT materials exhibit improved wetting properties toward water, although proper wetting of the untreated CNT was also achieved using alternative solvents for impregnation, such as ethanol or 1-propanol. Both for unfunctionalized and oxidized CNT and for all solvents considered in this study, drying of the impregnated material under a flow of nitrogen about 20 K below the boiling point of the solvent led to similarly sized supported Co_3O_4 nanoparticles of 3–6 nm. Using TEM, it was shown that clustering of Co_3O_4 nanoparticles was reduced using ethanol as a solvent for impregnation and even further using 1-propanol for the impregnation. These findings indicate that the nature of the solvent (a.o. surface tension) and drying conditions are more important for the preparation of well-dispersed and well-distributed supported cobalt oxide nanoparticles than the surface functionalization on its own.

The catalytic experiments at 20 bar showed that both for the systems on untreated and on oxidized CNT, the catalysts prepared by impregnation with solutions of cobalt nitrate in alcohols showed a superior cobalt-weight based activity over those prepared from an aqueous solution, because the cobalt particles had grown less during reduction and Fischer–Tropsch synthesis, leading to higher specific metal surface areas. These results emphasize the importance of avoiding clustering of supported nanoparticles by choosing an appropriate solvent and drying procedure. The distinctly higher surface-specific activity (TOF) for the catalysts supported on untreated CNT (TOF = 0.07 s^{-1} for Co particles larger than 6 nm) compared to functionalized CNT (TOF = 0.03 s^{-1} for particles larger than 6 nm) could not be explained by differences in cobalt dispersion or the degree of reduction. Although TPR suggests a retarded reduction of cobalt oxides to cobalt for the catalysts on oxidized CNT and despite the different reduction kinetics observed by XANES, the extent of reduction under steady state Fischer–Tropsch synthesis in all cases was very similar and very high and neither explains the differences in activity nor in selectivity. However, *in situ* XRD studies indicated that *hcp* Co was present for the catalysts on untreated CNT, while this was not the case for the catalysts on oxidized CNT, which rationalizes the superior activity of the catalysts on unmodified support materials.

While in terms of initial activity and selectivity of the catalysts, surface functionalization did not have a positive effect, gas-phase oxidation brought about a higher stability of the materials. While catalysts supported on untreated CNT displayed a substantial loss of activity that could be attributed to average cobalt particle growth. The catalysts supported on oxidized CNT maintained their catalytic activity, presumably due to a stronger anchoring of the cobalt nanoparticles to the support surface. These observations showed that the design of ideal Fischer–Tropsch catalysts remains a challenging tasks and that trade-offs have to be made in order to balance initial catalytic performance and long-term stability.

Acknowledgments

We gratefully acknowledge Shell Global Solutions for financial support. We also thank Jesper Sattler for carrying out Raman spectroscopy, Daniel Stellwagen for help with interpreting Raman spectra, and Rien van Zwienen for technical assistance on high-pressure catalytic testing. The Research Council of Norway is acknowledged for financial support through the SYNKNØYT program, and the personnel of the Swiss–Norwegian Beamlines (SNBL) at ESRF are highly acknowledged for experimental assistance.

Appendix A. Supplementary material

Supplementary data associated with this article can be found, in the online version, at http://dx.doi.org/10.1016/j.jcat.2014.12.010.

References

[1] M.E. Dry, Catal. Today 71 (2002) 227–241.
[2] J.L. Casci, C.M. Lok, M.D. Shannon, Catal. Today 145 (2009) 38–44.
[3] M.E. Dry, J. Chem. Technol. Biotechnol. 77 (2002) 43–50.
[4] M.E. Dry, Stud. Surf. Sci. Catal. 152 (2004) 533–600.
[5] E. Iglesia, Appl. Catal. A Gen. 161 (1997) 59–78.
[6] A.Y. Khodakov, W. Chu, P. Fongarland, Chem. Rev. 107 (2007) 1692–1744.
[7] Q. Zhang, J. Kang, Y. Wang, ChemCatChem 2 (2010) 1030–1058.
[8] B.H. Davis, Cobalt FT Catalysts, in: P.M. Maitlis, A. de Klerk (Eds.), Greener Fischer–Tropsch Process. Fuels Feestocks, first edit, 2013, pp. 193–207.
[9] W. Chu, P. Chernavskii, L. Gengembre, G. Pankina, P. Fongarland, A.Y. Khodakov, J. Catal. 252 (2007) 215–230.
[10] F. Diehl, A.Y. Khodakov, Oil Gas Sci. Technol. 64 (2009) 11–24.
[11] F. Morales, B.M. Weckhuysen, Promotion Effects in Co-based Fischer–Tropsch Catalysis, in: J.J. Spivey, K.M. Dooley (Eds.), Catal, vol. 19, The Royal Society of Chemistry, Cambridge, 2006, pp. 1–20.
[12] R. Oukaci, A.H. Singleton, J.G. Goodwin, Appl. Catal. A Gen. 186 (1999) 129–144.
[13] C.H. Bartholomew, R.C. Reuel, J. Catal. 85 (1984) 78–88.
[14] G. Jacobs, T.K. Das, Y. Zhang, J. Li, G. Racoillet, B.H. Davis, Appl. Catal. A Gen. 233 (2002) 263–281.
[15] J. van de Loosdrecht, S. Barradas, E.A. Caricato, N.G. Ngwenya, P.S. Nkwanyana, M.A.S. Rawat, B.H. Sigwebela, P.J. van Berge, J.L. Visagie, Top. Catal. 26 (2003) 121–127.
[16] T.O. Eschemann, J.H. Bitter, K.P. de Jong, Catal. Today 228 (2014) 89–95.
[17] J.P. den Breejen, P.B. Radstake, G.L. Bezemer, J.H. Bitter, V. Frøseth, A. Holmen, K.P. de Jong, J. Am. Chem. Soc. 131 (2009) 7197–7203.
[18] J.H. den Otter, K.P. de Jong, Top. Catal. 57 (2013) 445–450.
[19] C.M. Lok, Process for Preparing Cobalt Catalysts on Titania Support, EP 1 542 794 A1, 2010.

[20] S. Storsæter, Ø. Borg, E.A. Blekkan, B. Tøtdal, A. Holmen, Catal. Today 100 (2005) 343–347.
[21] E. Iglesia, S.L. Soled, R.A. Fiato, H.V. Grayson, J. Catal. 143 (1993) 345–368.
[22] A.R. de la Osa, A. De Lucas, A. Romero, J.L. Valverde, P. Sánchez, Catal. Today 176 (2011) 298–302.
[23] V.A. de la Peña O'Shea, M.C.Á. Galván, A.E. Prats Platero, J.M. Campos-Martin, J.L.G. Fierro, Chem. Commun. 47 (2011) 7131–7133.
[24] B. Jongsomjit, C. Sakdamnuson, J.G. Goodwin Jr., P. Praserthdam, Catal. Lett. 94 (2004) 209–215.
[25] S.J. Tauster, S.C. Fung, R.L. Garten, J. Am. Chem. Soc. 100 (1978) 170–175.
[26] G.L. Bezemer, U. Falke, A.J. van Dillen, K.P. de Jong, Chem. Commun. (Camb.) (2005) 731–733.
[27] P. Serp, M. Corrias, P. Kalck, Appl. Catal. A Gen. 253 (2003) 337–358.
[28] K.P. de Jong, J.W. Geus, Catal. Rev. 42 (2000) 481–510.
[29] H. Xiong, M.A.M. Motchelaho, M. Moyo, L.L. Jewell, N.J. Coville, J. Catal. 278 (2011) 26–40.
[30] H. Xiong, M.A.M. Motchelaho, M. Moyo, L.L. Jewell, N.J. Coville, Catal. Today 214 (2013) 50–60.
[31] F. Rodriguez-Reinoso, Carbon 36 (1998) 159–175.
[32] W. Xia, C. Jin, S. Kundu, M. Muhler, Carbon 47 (2009) 919–922.
[33] J.-P. Tessonnier, D. Rosenthal, T.W. Hansen, C. Hess, M.E. Schuster, R. Blume, F. Girgsdies, N. Pfänder, O. Timpe, D.S. Su, R. Schlögl, Carbon 47 (2009) 1779–1798.
[34] G.L. Bezemer, P.B. Radstake, V. Koot, A.J. van Dillen, J.W. Geus, K.P. de Jong, J. Catal. 237 (2006) 291–302.
[35] T.G. Ros, A.J. van Dillen, J.W. Geus, D.C. Koningsberger, Chemistry (Easton) 8 (2002) 1151–1162.
[36] R.W. Gosselink, R. van den Berg, W. Xia, M. Muhler, K.P. de Jong, J.H. Bitter, Carbon 50 (2012) 4424–4431.
[37] V. Likodimos, T.A. Steriotis, S.K. Papageorgiou, G.E. Romanos, R.R.N. Marques, R.P. Rocha, J.L. Faria, M.F.R. Pereira, J.L. Figueiredo, A.M.T. Silva, P. Falaras, Carbon 69 (2014) 311–326.
[38] U.M. Graham, G. Jacobs, M.K. Gnanamani, S.M. Lipka, W. Shafer, C.R. Swartz, T. Jermwongratanachai, R. Chen, F. Rogers, B.H. Davis, ACS Catal. 4 (2014) 1662–1672.
[39] T. Fu, Z. Li, Catal. Commun. 47 (2014) 54–57.
[40] T. Fu, R. Liu, J. Lv, Z. Li, Fuel Process. Technol. 122 (2014) 49–57.
[41] Y. Yang, L. Jia, B. Hou, D. Li, J. Wang, Y. Sun, J. Phys. Chem. C 118 (2014) 268–277.
[42] T. Fu, Y. Jiang, J. Lv, Z. Li, Fuel Process. Technol. 110 (2013) 141–149.
[43] A. Karimi, B. Nasernejad, A.M. Rashidi, A. Tavasoli, M. Pourkhalil, Fuel 117 (2014) 1045–1051.
[44] Z. Yu, Ø. Borg, D. Chen, E. Rytter, A. Holmen, Top. Catal. 45 (2007) 69–74.
[45] G. Prieto, J. Zečević, H. Friedrich, K.P. de Jong, P.E. de Jongh, Nat. Mater. 12 (2013) 34–39.
[46] P. Munnik, P.E. de Jongh, K.P. de Jong, J. Am. Chem. Soc. 136 (2014) 7333–7340.
[47] D. Schanke, S. Vada, E.A. Blekkan, A.M. Hilmen, A. Hoff, A. Holmen, J. Catal. 156 (1995) 85–95.
[48] N.E. Tsakoumis, R. Dehghan, R.E. Johnsen, A. Voronov, W. van Beek, J.C. Walmsley, Ø. Borg, E. Rytter, D. Chen, M. Rønning, A. Holmen, Catal. Today 205 (2013) 86–93.
[49] T.I.T. Okpalugo, P. Papakonstantinou, H. Murphy, J. McLaughlin, N.M.D. Brown, Carbon 43 (2005) 153–161.
[50] S. Kundu, Y. Wang, W. Xia, M. Muhler, J. Phys. Chem. C 112 (2008) 16869–16878.
[51] A. Sadezky, H. Muckenhuber, H. Grothe, R. Niessner, U. Pöschl, Carbon 43 (2005) 1731–1742.
[52] Y. Wang, D.C. Alsmeyer, R.L. McCreery, Chem. Mater. 2 (1990) 557–563.
[53] P. Li, J. Liu, N. Nag, P.A. Crozier, J. Phys. Chem. B 109 (2005) 13883–13890.
[54] T. Fu, C. Huang, J. Lv, Z. Li, Fuel 121 (2014) 225–231.
[55] E.W. Kuipers, I.H. Vinkenburg, H. Oosterbeek, J. Catal. 152 (1995) 137–146.
[56] S. Rane, Ø. Borg, J. Yang, E. Rytter, A. Holmen, Appl. Catal. A Gen. 388 (2010) 160–167.
[57] S. Rane, Ø. Borg, E. Rytter, A. Holmen, Appl. Catal. A Gen. 437–438 (2012) 10–17.
[58] D.B. Bukur, Z. Pan, W. Ma, G. Jacobs, B.H. Davis, Catal. Lett. 142 (2012) 1382–1387.
[59] L. Braconnier, E. Landrivon, I. Clémençon, C. Legens, F. Diehl, Y. Schuurman, Catal. Today 215 (2013) 18–23.
[60] J.-X. Liu, H.-Y. Su, D.-P. Sun, B.-Y. Zhang, W.-X. Li, J. Am. Chem. Soc. 135 (2013) 16284–16287.